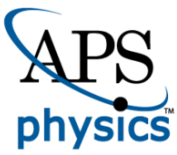

Electromagnon Resonance at Room Temperature with Gigantic Magnetochromism

H. Shishikura, Y. Tokunaga, Y. Takahashi, R. Masuda, Y. Taguchi, Y. Kaneko, and Y. Tokura

Phys. Rev. Applied **9**, 044033 — Published 23 April 2018

DOI: 10.1103/PhysRevApplied.9.044033

Electromagnon resonance at room temperature with gigantic magnetochromism

H. Shishikura[1], Y. Tokunaga[2,3], Y. Takahashi[1,2,4]*, R. Masuda[1], Y. Taguchi[2], Y. Kaneko[2], Y. Tokura[1,2]

[1]*Department of Applied Physics and Quantum Phase Electronics Center (QPEC), University of Tokyo, Tokyo 113-8656, Japan*

[2]*RIKEN Center for Emergent Matter Science (CEMS), Wako, Saitama 351-0198, Japan*

[3]*Department of Advanced Materials Science, University of Tokyo, Kashiwa 277-8561, Japan*

[4]*PRESTO, Japan Science and Technology Agency (JST), Chiyoda-ku, Tokyo 102-0075, Japan.*

* youtarou-takahashi@ap.t.u-tokyo.ac.jp

Abstract

Elementary excitation characteristic of the magnetoelectric (ME) multiferroics is a magnon endowed with the electric activity, which is referred to as electromagnon. The electromagnon resonance mediated by the bilinear exchange coupling potentially exhibits the strong terahertz light-matter interaction with novel optical properties different from the conventional magnon excitation. Here we report the robust electromagnon resonance on the helimagnetic Y-type hexaferrites in a wide temperature range including room temperature. Furthermore, the efficient magnetic-field controls of the electromagnon are demonstrated on the flexible spin structure of these compounds, leading to the generation/annihilation of the resonance as well as the large resonance energy shift. These terahertz characteristics of the electromagnon exemplify the versatile magneto-optical functionality driven by the ME coupling in the multiferroics, paving a way for possible terahertz applications as well as terahertz control of a magnetic state of matter.

I. Introduction

Magnetoelectric (ME) coupling, which is a cross-coupling between the magnetism and electric properties, has attracting increasing attention in condensed matter physics including topological insulator, spintronics and ME multiferroics [1,2]. The ME coupling produces diverse light-matter interactions through the couplings between the ac/dc electric and magnetic responses as exemplified by the optical ME effect [1]. The multiferroics exhibit not only the strong mutual coupling between the magnetic orders and ferroelectricity [3,4], but also unique composite excitations of the spin degrees of freedom and electronic lattice, which in turn lead to a magnon excitation endowed with electric activity referred to as electromagnon [5-7]. The electromagnon resonance potentially gives rise to the strong optical response in the terahertz region with novel functionalities controlled by external fields, whereas these properties remain elusive. In addition, these flexible optical properties of the electromagnon at room temperature may provide a promising approach for the possible applications in terahertz technologies, which are still at a development stage in spite of the strong demand for applications [8-10].

Since the particular spin orders produce the ferroelectricity in the multiferroics, the mutual control of them, *i.e.* the magnetic field control of the ferroelectricity [11,12] as well as the electric field control of magnetism [13,14], have been demonstrated. Accordingly, the fluctuation of the spin orders always possesses the electric counterpart, leading to the electromagnon resonance, which can be viewed as the elementary excitation unique to the multiferroics. The helical spin orders ensure the presence of ferroelectricity through the spin-current mechanism; the local electric polarization is proportional to $e_{ij}\times(S_i\times S_j)$, where e_{ij} is an unit vector connecting adjacent spins S_i and S_j [15-17]. Accordingly, the cycloidal helical spin structure produces macroscopic electric

polarization, which in turn leads to the concomitant electromagnon excitation [5,7]. In fact, the electromagnon resonance has been reported as a strong far-infrared absorption on the helical spin phase of multiferroic $TbMnO_3$ [6]. Contrary to the ferroelectricity driven by spin-current mechanism, there are another type of electromagnon resonance whose origin is ascribed to the exchange striction (ES) mechanism, in which the electric activity is generated by the lattice-coupled spin exchange interaction [18]. The electromagnon driven by the ES mechanism exhibits the remarkable characteristics including the higher resonance energy and the even stronger optical response. Since the specific symmetries of the chemical and/or magnetic lattice fold the magnon branch, the optical transition is allowed for the magnon at the zone edge in the magnetic Brillouin zone. This is because the ES electromagnon has the higher resonance energy. The effective field on each spin, which arises from the ES, gives rise to the one magnon excitation only for the noncollinear spin structures including the helical spin one. Since the ES mechanism causes the strong effective field because of the generic coupling to optical phonons, the optical response of the electromagnon is a few orders of magnitude higher than conventional magnon resonance, as reported in several helical magnets [19,20].

Hexaferrite compounds investigated here are promising materials hosting the strong ME coupling driven by the helical spin structures in a wide temperature range including room temperature [12,21-23]. The electromagnon resonance has been reported for the helical spin phases of Y- and Z-type hexaferrites at lower temperatures [24-26]. These electromagnon resonances have been ascribed to the ES mechanism, because the light polarization to excite the electromagnon resonance is always parallel to the crystallographic *c* axis irrespective of the detail of the helical spin structures. The inelastic neutron study has confirmed that the energy of magnon at the zone edge

coincides with the resonance energy of the electromagnon observed by the terahertz spectroscopy on Y-type hexaferrite $Ba_2Mg_2Fe_{12}O_{22}$ [27]. Similar characteristics has been reported on the perovskite-$R$$MnO_3$ [18] and $R$$Mn_2O_5$ [28] (R-rare earth ion); the ferroelectricity is derived from the spin-current mechanism, while the ES mechanism is responsible for the electromagnon resonance. Because of the existence of various helical spin phases including at room temperature, the Y-type hexaferrites potentially exhibit the electromagnon resonance at room temperature and provide flexible control of the optical responses by the external field.

Here we target the terahertz electromagnon resonance and the versatile magnetic field controls of electromagnon including at room temperature for Y-type hexaferrites with two compositions. The helical spin phases of $BaSrCo_2Fe_{11}AlO_{22}$[29] shows the robust electromagnon resonance at zero field, which is suppressed owing to the transition from the helical spin phase to the collinear ferrimagnetic phase by application of magnetic field. On the other hand, the external magnetic field generates the electromagnon resonance in $Ba_{0.5}Sr_{1.5}Cu_2Fe_{11}AlO_{22}$, whereas the resonance is absent at zero field. A steep evolution of the electromagnon resonance as well as its gigantic energy shift is demonstrated in this compound by applying the magnetic field.

II. Method

Single crystals of $BaSrCo_2Fe_{11}AlO_{22}$ and $Ba_{0.5}Sr_{1.5}Cu_2Fe_{11}AlO_{22}$ were grown by a high oxygen-pressure (10 atm) laser floating zone method [30]. These samples were characterized by the measurements of magnetization (see Fig. 2(d), Fig. 3(e), Fig. 4(e) and Supplemental Material [31]). The typical dimensions of samples are $3 \times 3 \times 0.2$ mm^3.

We employed the time-domain terahertz spectroscopy for the optical measurements

from 1.5 meV to 8 meV. The laser pulses with duration of 100 fs from a mode-locked Ti: sapphire laser were split into two paths to generate and detect the terahertz pulses. The terahertz pulses were generated in ZnTe crystal by the optical rectification effect. The waveform of the terahertz pulses were measured by a dipole antenna. The linearly polarized terahertz light was prepared by the wire-grid polarizers. The magnetic field from a superconducting magnet was applied perpendicular to the propagation vector of the terahertz pulses, *i.e.* in Voigt geometry, so that the Faraday rotation was avoided in this experiment.

III. Results

A. Fundamental properties of $BaSrCo_2Fe_{11}AlO_{22}$ and $Ba_{0.5}Sr_{1.5}Cu_2Fe_{11}AlO_{22}$

In this experiment, the terahertz optical responses of the Y-type hexaferrites $BaSrCo_2Fe_{11}AlO_{22}$ and $Ba_{0.5}Sr_{1.5}Cu_2Fe_{11}AlO_{22}$ were measured. The magnetic system of Y-type hexaferrites consist of the ferrimagnetic L- and S-blocks stacking alternately along the *c* axis (Fig. 1(a)); each L- and S-block can be viewed as possessing the large and small classical moments, respectively [23,32,33]. These L- and S-spins form various helical spin structures as shown in Figs. 1(b)-1(d). For example, the alternating longitudinal conical (ALC) structure is reported for several Y-type compounds; the L-spins have antiferromagnetic component along the *c* axis in addition to the longitudinal helical structure for the in-plane components (Fig. 1(b)) [30,34,35]. In the magnetic field along the *c* axis (H_{dc}//c), the ALC spin structure turns into the longitudinal conical (LC) one, whose *c* axis components of L-spins are ferromagnetically ordered, while keeping the helical spin components for the in-plane (Fig. 1(c)). In the higher magnetic field, the collinear ferrimagnetic (FM) structure takes place. On the other hand, the magnetic field applied perpendicular to the *c* axis ($H_{dc}\perp c$) gives rise to

the transvers conical (TC) structure (Fig. 1(d)), where the spin-cycloid plane emerges in addition to the ferrimagnetic components. The spin-cycloid components in the TC structure always produces the ferroelectric polarization driven by the spin-current mechanism as reported in various hexaferrites compounds, including at room temperature [12,21-23]. With increasing the magnetic field, the cone angle gradually closes, and subsequently the collinear FM structure takes place while extinguishing the ferroelectric polarization. The phase diagrams are summarized for the $BaSrCo_2Fe_{11}AlO_{22}$ (Figs. 1(e) and 1(f)) and for the $Ba_{0.5}Sr_{1.5}Cu_2Fe_{11}AlO_{22}$ (Figs. 1(g) and 1(h)) (see also the supplementary material). The ALC spin structure is more stable in the $Ba_{0.5}Sr_{1.5}Cu_2Fe_{11}AlO_{22}$, while it is a metastable state except for the intermediate temperature region for the $BaSrCo_2Fe_{11}AlO_{22}$ [30].

B. Terahertz electromagnon resonance for $BaSrCo_2Fe_{11}AlO_{22}$

The characteristics of the electromagnon resonance for the $BaSrCo_2Fe_{11}AlO_{22}$ are summarized in Fig. 2. The temperature dependence of the imaginary part of dielectric constant ε_2 shows the presence of the distinct resonance in the terahertz region (1 THz ~ 4.1 meV) as shown in the Fig. 2(a). The resonance structure is observed for the light polarized parallel to the *c* axis ($E^{\omega}//c$, $H^{\omega}\perp c$), whereas the spectra for other polarizations ($E^{\omega}\perp c$, $H^{\omega}//c$ and $E^{\omega}\perp c$, $H^{\omega}\perp c$) show merely the tail of the higher-lying optical phonons of little temperature dependence. The observed polarization selection rule clearly indicates the presence of the electric transition-dipole polarized parallel to the *c* axis ($E^{\omega}//c$), consistent with the earlier works on the helical spin phase of the Y-type hexaferrite $Ba_2Mg_2Fe_{12}O_{22}$ [24]. The resonance peak shifts the energy from ~3.5 meV (300 K) to ~6 meV (150 K) and the peak intensity develops from 2.5 (300 K) to 6 (150 K) in ε_2 as the temperature decreases (Fig. 2(a)). This peak shift is consistent with the

results of the inelastic neutron scattering study on the zone-edge magnon for $BaSrCo_2Fe_{11}AlO_{22}$ [30]. Thus the observed electrically active excitation can be ascribed to the electromagnon resonance driven by the ES mechanism.

The correlation between the spin structures and the electromagnon resonance was studied under the magnetic field ($H_{dc} \perp c$) at 200 K (Figs. 2(b) and 2(e)) and 300 K (Figs. 2(c) and 2(f)). At 200 K, the electromagnon resonance is observed at ~6 meV with little magnetic field dependence below 2 T, where the magnetic field reduces the cone angle of the TC spin structure as suggested by the increase of magnetization (Fig. 2(d)). The decrease of the peak intensity and the peak shift to low energy are observed upon the transition to the FM phase around 2 T (triangles in Figs. 2(d) and 2(e)). In the collinear FM phase (> 2 T), the spectral intensity of electromagnon decreases and disappears above 4 T. These results manifest a decisive role of the noncollinear helical spin structure in the electromagnon activity, as expected for the ES-driven electromagnon.

The ALC structure is stable at the vicinity of zero field at 300 K (Fig. 1(f)), which is turned into the TC structure by a magnetic field lower than 0.1 T as manifested by the hysteretic behavior of the magnetization curve (inset to Fig. 2(d)). The ALC spin structure gives rise to the clear electromagnon resonance at 3.5 meV (300 K, 0 T). Upon the transition from the ALC phase to the TC phase, the resonance energy leaps from 3.5 meV to 4 meV as shown in Figs. 2(c) and 2(f). As the magnetic field is further increased, the electromagnon resonance gradually decreases in intensity around the transition at 1.9 T (triangles in Figs. 2(d) and 2(f)) and no resonance peak is discerned above 4 T. Therefore, it is indicated that the helical spin structures including the ALC and the TC in the Y-type hexaferrites produce the robust electromagnon resonance and the transitions between these helical spin phases and the collinear FM phase exhibit the strong magnetochromism in a wide temperature range including room temperature.

C. Steep magnetochromism on the phase transition in $Ba_{0.5}Sr_{1.5}Cu_2Fe_{11}AlO_{22}$

One way of efficient control for magnetochromism is the use of a sharp magnetic transition. The magnetic field along the *c* axis ($H_{dc}//c$) causes a spin-flop like transition from the ALC phase to the LC phase for $Ba_{0.5}Sr_{1.5}Cu_2Fe_{11}AlO_{22}$ (see the phase diagram in Fig. 1(g) and the magnetization curves in Fig. 3(e)); the antiferromagnetic *c* axis components of L-spins turn into the ferromagnetic one around 2 T, while keeping helical spin component for in-plane. The magnetization plateau below the transition (< 2 T) indicates a small cone angle of ALC structure for $Ba_{0.5}Sr_{1.5}Cu_2Fe_{11}AlO_{22}$, resulting in a small amount of helical spin component and dominant antiferromagnetic one (see inset to Fig. 3(a)).

Figure 3 summarizes the characteristics of electromagnon for $Ba_{0.5}Sr_{1.5}Cu_2Fe_{11}AlO_{22}$ under the magnetic field ($H_{dc}//c$). No peak structure is discerned in the ALC phase (< 2 T) at 200 K (Figs. 3(a) and 3(f)). (We will discuss later why the electromagnon is inactive in the ALC phase of $Ba_{0.5}Sr_{1.5}Cu_2Fe_{11}AlO_{22}$.) With increasing the magnetic field through the phase transition at 2 T (indicated by triangles in Figs. 3(e) and 3(f)), however, the resonance peak for $E^{\omega}//c$ abruptly appears around 4 meV and then shows a steep variation (see the supplementary material for the polarization dependence): The peak structure starts to rise from 1.95 T and shows a maximum at 2.05 T, manifesting the dramatic magnetochromism driven by the generation of electromagnon. Further increase of magnetic field causes monotonous decrease of the electromagnon spectral intensity, and no resonances structure is observed above 4.5 T, as shown in Figs. 3(b) and 3(f). The suppression of the electromagnon can be explained by the decrease of the helical spin component, which is suggested by the increase of the magnetization above the spin-flop like transition (> 2 T). In addition, the remarkable energy shift is

observed from 4 meV (2.05 T) to 2.5 meV (3 T).

Similar magnetic field dependence is observed even at 300 K as shown in Figs. 3(c), 3(d) and 3(g). There is discerned no resonance peak at 0 T (Fig. 3(c)). With increasing the magnetic field through the transition from the ALC phase to the LC phase around 2 T (triangles in Figs. 3(e) and 3(g)), the electromagnon resonance develops around 3 meV and shows a maximum at 2.5 T. Further increase of the magnetic field reduces the electromagnon resonance with a peak shift to low energy (Figs. 3(d) and 3(g)), and no resonance structure is observed above 4 T.

D. Gigantic energy shift of the electromagnon resonance in transverse conical (TC) phase of $Ba_{0.5}Sr_{1.5}Cu_2Fe_{11}AlO_{22}$

Modest magnetic field applied perpendicular to the *c* axis ($H_{dc} \perp c$) stabilizes the TC phase (see the phase diagram in Fig. 1(h)). The electromagnon resonance shows a distinct behavior in the TC phase as follows. There is no resonance structure at 0 T again (Figs. 4(a) and 4(c)). At 200 K, the peak intensity of electromagnon gradually develops with increasing the magnetic field (Fig. 4(a)), where the cone angle gradually decreases as evidenced by the monotonous increase of the magnetization (see insets to Figs. 4(c) and 4(e)). One remarkable feature of the present electromagnon is a large energy shift with the magnetic field; the resonance energy of 2 meV (1 T) continuously shifts to 5 meV (3.8 T) with an evolution of the resonance peak (Figs. 4(a) and 4(f)). The peak intensity and resonance energy of electromagnon are simultaneously maximized at 3.8 T. The phase transition to the FM phase at 4.2 T is manifested by the kink structure in the magnetization curves (indicated with triangles in Fig. 4(e)). Above this transition, the electromagnon resonance rapidly diminishes with a peak shift to low energy as shown in Figs. 4(b) and 4(f). No clear resonance is seen in the

collinear FM phase above 5 T.

The electromagnon resonance shows the similar magnetic field dependence also at 300 K (Figs. 4(c), 4(d) and 4(g)). The magnetic field induces the development of the electromagnon resonance with a shift to higher energy. The electromagnon shows the maximum at 3.8 T with the peak magnitude of 3.3 in ε_2 at 3.3 meV (Figs. 4(c) and 4(g)). Further increase of the magnetic field rapidly suppresses the electromagnon resonance (Figs. 4(d) and 4(g)). There is no resonance in terahertz region above 5 T.

IV. Discussions

Our experiments demonstrate the magnetic-field control of the resonance energy and the magnitude of the electromagnon resonance, including at room temperature. The observed electromagnon is always active for the light polarized parallel to the *c* axis for both $BaSrCo_2Fe_{11}AlO_{22}$ and $Ba_{0.5}Sr_{1.5}Cu_2Fe_{11}AlO_{22}$ irrespective of the detail of the helical spin structures, consistent with the earlier works on Y-type hexaferrite $Ba_2Mg_2Fe_{12}O_{22}$ [24,25]. Accordingly, it is concluded that this polarization selection rule of the electromagnon ($E^{\omega}//c$) is a common character for the Y-type hexaferrites, which in turn confirms that the ES mechanism is responsible for the electromagnon activity in the hexaferrite family.

The ALC phase for $Ba_{0.5}Sr_{1.5}Cu_2Fe_{11}AlO_{22}$ (Fig. 3) shows the absence of the distinct resonance peak, whereas the other helical spin structures including the ALC phase for $BaSrCo_2Fe_{11}AlO_{22}$ (Fig. 2) exhibit the electromagnon resonances. The suppression of the electromagnon resonance for $Ba_{0.5}Sr_{1.5}Cu_2Fe_{11}AlO_{22}$ can be explained by a lack of the helical spin component *i.e.* the ALC spin structure with closed cone angle. In contrast, the opened spin-cone for the ALC spin structure in the $BaSrCo_2Fe_{11}AlO_{22}$ is suggested by a monotonous increase of the magnetization for $H_{dc}//c$ (see supplementary materials).

The appreciable amount of the helical spin component for the ALC phase in the $BaSrCo_2Fe_{11}AlO_{22}$ results in the clear electromagnon resonance. Therefore, the helical spin components for each spin structure plays a crucial role for the electromagnon activity.

The spectral weights of the electromagnon (ΔSW in Fig. 5) also clearly demonstrate the field dependent variation of the electromagnon. The ΔSW are calculated as the integral of the $\varepsilon_0\varepsilon_2\omega$ between 1.6 and 7 meV after the subtraction of the background consisting of the low energy tail of the optical phonons (see the spectra in Fig. 2, 3 and 4). The sudden increase of the ΔSW at 2 T for LC phase of the $Ba_{0.5}Sr_{1.5}Cu_2Fe_{11}AlO_{22}$ ($H_{dc}//c$, open squares) is contrasted with the rather continuous but larger amplitude of the magnetic field dependence in TC phase ($H_{dc}\perp c$, closed triangles). The ΔSW of the $BaSrCo_2Fe_{11}AlO_{22}$ shows monotonous decrease above 1 T (Fig. 5(a) and (b)). The maximum ΔSW of the $Ba_{0.5}Sr_{1.5}Cu_2Fe_{11}AlO_{22}$ in $H_{dc}\perp c$ (closed triangles) is as large as that of the $BaSrCo_2Fe_{11}AlO_{22}$ (open circles) at 200 K (Fig. 5(a)), whereas the field-induced electromagnon in $H_{dc}//c$ (open squares) shows a half of these ΔSWs. At 300 K, the difference in the spectral weights tends to decrease as shown in Fig. 5(b).

The strong magnetic field dependence of the electromagnon resonance energy is observed in the LC phase and the TC phase for $Ba_{0.5}Sr_{1.5}Cu_2Fe_{11}AlO_{22}$ as shown in Figs. 3 and 4, respectively. In the TC phase, the magnetic-field gradient of the resonance energy at 200 K is as large as +1.3 meV T^{-1} in between 1 T and 3 T (Fig. 4), while it shows a value of –1.2 meV T^{-1} for the LC phase in between 2 T and 3 T (Fig. 3). These energy shifts induced by the magnetic field are remarkably larger than the conventional Zeeman shift for magnon: $\mu_B g$ = 0.116 meV T^{-1}, where μ_B is Bohr magneton and g = 2 is the g-factor for free electron. Because the present electromagnon is the excitation at the zone edge in the magnetic Brillion zone, the change of the magnon dispersion is

mainly responsible for that of the electromagnon resonance energy. In $Ba_{0.5}Sr_{1.5}Cu_2Fe_{11}AlO_{22}$, a continuous deformation of the spin structure induced by the external magnetic field likely modifies the magnon branches, which in turn leads to the large energy shift of the electromagnon. One possible explanation is a continuous variation of the magnetic modulation vector q_m of the helical structures, which simultaneously modifies the magnon dispersion, *i.e.* the resonance energy of the electromagnon at the zone edge. (Here the q_m represents the c axis component of the magnetic modulation vector $(0,0,q_m)$ for a conventional hexagonal unit cell [30].) In fact, the strong q_m dependence of the electromagnon resonance has been reported for the helical spin phases of perovskite-RMnO$_3$ by the systematic composition control [36]. The temperature-dependent continuous variation of q_m has been observed on the Y-type hexaferrites by the neutron scattering measurements [30,33,34]. The variation of q_m induced by magnetic field is also reported for $Ba_2Mg_2Fe_{12}O_{22}$ [37]. Such flexibility of q_m may work positively for the magnetic-field control of the electromagnon characteristics. The little magnetic field dependence of the electromagnon in the TC phase for the $BaSrCo_2Fe_{11}AlO_{22}$ can be explained by the commensurate locking of q_m=1.5 in the TC phase (see Figs. 2(e) and 2(f)) [30]. Recently, the energy shift of the ES-driven electromagnon in the magnetic field (0.2 T) was reported on the Z-type hexaferrite below 200 K, while the remanent spectral weights were observed at higher temperatures [38]. The possible contribution of the Dzyaloshinskii-Moriya interaction to the resonance energy of the electromagnon, which was assumed to appear due to the symmetry-lowering in the ferroelectric TC phase, was suggested by the calculation based on the block spin model including the L- and S-spins. Although for the Y-type hexaferrites the Dzyaloshinskii-Moriya interaction may similarly affect the energy shift of the electromagnon on the TC phases in the magnetic field $H_{dc} \perp c$ (Fig. 2 and 4), the

field- and composition-dependent variations of the spin structures would play a dominant role in the gigantic magnetochromism and the remarkable difference between $Ba_{0.5}Sr_{1.5}Cu_2Fe_{11}AlO_{22}$ and $BaSrCo_2Fe_{11}AlO_{22}$.

In conclusion, we have demonstrated the terahertz electromagnon resonances driven by the ES mechanism on the helical spin phases of Y-type hexaferrites with two compositions ($BaSrCo_2Fe_{11}AlO_{22}$ and $Ba_{0.5}Sr_{1.5}Cu_2Fe_{11}AlO_{22}$), including at room temperature. The $BaSrCo_2Fe_{11}AlO_{22}$ shows the robust electromagnon resonance at zero field, which vanishes in the collinear FM phase under the magnetic field. The magnetic phase transition from the ALC phase to the LC phase generates the electromagnon resonance in $Ba_{0.5}Sr_{1.5}Cu_2Fe_{11}AlO_{22}$, which leads to the gigantic magnetochromism. The large magnetic field dependence of the electromagnon in energy and magnitude is demonstrated on the LC and TC phases of $Ba_{0.5}Sr_{1.5}Cu_2Fe_{11}AlO_{22}$ as well, enabling the efficient magnetic field control of terahertz absorption. The strong electromagnon resonances and versatile magnetic variations of the optical responses caused by the flexible helical spin structures of the hexaferrites may promise the utilization of strong terahertz light-matter interactions under external control. The magnetically tunable terahertz absorber is a possible application of Y-type hexaferrites, in analogy to the broadly used microwave absorber utilizing the ferromagnetic resonance. The electromagnon excitation in the ferrimagnetic TC and LC phases potentially enables the generation of the magnon spin-current and the ultrafast spin injection by the irradiation of the terahertz wave, which would be applied to the terahertz-voltage conversion [39]. The resonant excitation of electromagnons by a coherent terahertz source can provide a promising approach to the ultrafast control of magnetism within a few picosecond with generating little excess energy [40].

Acknowledgements

This work has been supported by the JST through Grant No. JPMJPR1423 and JPMJCR16F1, and by JSPS KAKENHI (Grant No. 24224009, No. 17H04845 and 17K19050).

H. S., R. M. and Y. Takahashi carried out the optical spectroscopy. Y. Tokunaga, Y. Taguchi and Y. K. prepared the single crystalline samples. The results were discussed and interpreted by Y. Takahashi, H. S., Y. Tokunaga and Y. Tokura.

Reference

[1] F. Matsukura, Y. Tokura and H. Ohno, *Control of magnetism by electric fields,* Nat. Nanotech. **10**, 209 (2015).

[2] M. K. Hasan and C. L. Kane, *Colloquium: Topological insulators*, Rev. Mod. Phys. **82**, 3045 (2010).

[3] W. Eerenstein, N. D. Mathur and J. F. Scott, *Multiferroic and magnetoelectric materials,* Nature **442**, 759 (2006).

[4] Y. Tokura, S. Seki and N. Nagaosa, *Multiferroics of spin origin,* Rep. Prog. Phys. **77**, 076501 (2014).

[5] H. Katsura, A. V. Balatsky and N. Nagaosa, *Dynamical magnetoelectric coupling in helical magnets,* Phys. Rev. Lett. **98**, 027203 (2007).

[6] A. Pimenov, A. A. Mukhin, V. Yu. Ivanov, V. D. Travkin, A. M. Balbashov and A. Loidl, *Possible evidence for electromagnons in multiferroic manganites,* Nat. Phys. **2**, 97 (2006).

[7] Y. Takahashi, R. Shimano, Y. Kaneko, H. Murakawa and Y. Tokura, *Magnetoelectric resonance with electromagnons in a perovskite helimagnet,* Nat. Phys. **8**, 121 (2011).

[8] T. Kleine-Ostmann, and T. Nagatsuma, *A review on terahertz communications*

research, J. Infrared Millim, Terahertz Waves **32**, 143 (2011).

[9] S. Koenig, D. Lopez-Diaz, J. Antes, F. Boes, R. Henneberger, A. Leuther, A. Tessmann, R. Schmogrow, D. Hillerkuss, R. Palmer, T. Zwick, C. Koos, W. Freude, O. Ambacher, J. Leuthold and I. Kallfass*, Wireless sub-THz communication system with high data rate*, Nat. Photonics. **7**, 977 (2013).

[10] Y.-C. Shen, *Terahertz pulsed spectroscopy and imaging for pharmaceutical applications: a review,* Int. J. Pharm. **417**, 48 (2011).

[11] T. Kimura, T. Goto, H. Shintani, K. Ishizaka, T. Arima and Y. Tokura*, Magnetic control of ferroelectric polarization,* Nature **426**, 55 (2003).

[12] S. Ishiwata, Y. Taguchi, H. Murakawa, Y. Onose and Y. Tokura*, Low-magnetic-field control of electric polarization vector in a helimagnet,* Science **319**, 1643 (2008).

[13] Y. Tokunaga, N. Furukawa, H. Sakai, Y. Taguchi, T. Arima and Y. Tokura*, Composite domain walls in a multiferroic perovskite ferrite,* Nat. Mater. **8**, 558 (2009).

[14] Y. S. Chai, S. Kwon, S. H. Chun, I. Kim, B.-G. Jeon, K. H. Kim and S. Lee*, Electrical control of large magnetization reversal in a helimagnet,* Nat. Commun. **5,** 4208 (2014).

[15] H. Katsura, N. Nagaosa and A. V. Balatsky, *Spin current and magnetoelectric effect in noncollinear magnets,* Phys. Rev. Lett. **95**, 057205 (2005).

[16] I. A. Sergienko and E. Dagotto, *Role of the Dzyaloshinskii-Moriya interaction in multiferroic perovskites,* Phys. Rev. B 73, 094434 (2006).

[17] M. Mostovoy, *Ferroelectricity in spiral magnets,* Phys. Rev. Lett. 96, 067601 (2006).

[18] R. Valdés Aguilar, M. Mostovoy, A. B. Sushkov, C. L. Zhang, Y. J. Choi, S-W. Cheong and H. D. Drew*, Origin of electromagnon excitations in multiferroic $RMnO_3$,* Phys. Rev. Lett. **102**, 047203 (2009).

[19] R. Valdés Aguilar, A. B. Sushkov, C. L. Zhang, Y. J. Choi, S.-W. Cheong and H. D. Drew, *Colossal magnon-phonon coupling in multiferroic $Eu_{0.75}Y_{0.25}MnO_3$,* Phys. Rev. B

76, 060404(R) (2007).

[20] Y. Takahashi, Y. Yamasaki, N. Kida, Y. Kaneko, T. Arima, R. Shimano and Y. Tokura, *Far-infrared optical study of electromagnons and their coupling to optical phonons in* $Eu_{1-x}Y_xMnO_3$ *(x=0.1, 0.2, 0.3, 0.4, and 0.45),* Phys. Rev. B **79**, 214431 (2009).

[21] T. Kimura, G. Lawes and A. P. Ramirez, *Electric Polarization Rotation in a Hexaferrite with Long-Wavelength Magnetic Structures,* Phys. Rev. Lett. **94**, 137201 (2005).

[22] Y. Kitagawa, Y. Hiraoka, T. Honda, T. Ishikura, H. Nakamura and T. Kimura*, Low-field magnetoelectric effect at room temperature.* Nat. Mater. **9**, 797 (2010).

[23] T. Kimura, *Magnetoelectric hexaferrites,* Annu. Rev. Condens. Matter Phys. **3**, 93 (2012).

[24] N. Kida, D. Okuyama, S. Ishiwata, Y. Taguchi, R. Shimano, K. Iwasa, T. Arima and Y. Tokura, *Electric-dipole-active magnetic resonance in the conical-spin magnet* $Ba_2Mg_2Fe_{12}O_{22}$*,* Phys. Rev. B **80**, 220406(R) (2009).

[25] N. Kida, S. Kumakura, S. Ishiwata, Y. Taguchi and Y. Tokura*, Gigantic terahertz magnetochromism via electromagnons in the hexaferrite magnet* $Ba_2Mg_2Fe_{12}O_{22}$*,* Phys. Rev. B **83**, 064422 (2011).

[26] F. Kadlec, C. Kadlec, J. Vít, F. Borodavka, M. Kempa, J. Prokleška, J. Buršík, R. Uhrecký, S. Rols, Y. S. Chai, K. Zhai, Y. Sun, J. Drahokoupil, V. Goian and S. Kamba*, Electromagnon in the Z-type hexaferrite* $(Ba_xSr_{1-x})_3Co_2Fe_{24}O_{41}$*,* Phys. Rev. B **94**, 024419 (2016).

[27] T. Nakajima, Y. Takahashi, S. Kibayashi, M. Matsuda, K. Kakurai, S. Ishiwata, Y. Taguchi, Y. Tokura and T. Arima*, Electromagnon excitation in the field-induced noncollinear ferrimagnetic phase of* $Ba_2Mg_2Fe_{12}O_{22}$ *studied by polarized inelastic neutron scattering and terahertz time-domain optical spectroscopy,* Phys. Rev. B **93**,

035119 (2016).

[28] J.-H. Kim, M. A. van der Vegte, A. Scaramucci, S. Artyukhin, J.-H. Chung, S. Park, S.-W. Cheong, M. Mostovoy and S.-H. Lee, *Magnetic Excitations in the Low-Temperature Ferroelectric Phase of Multiferroic YMn_2O_5 Using Inelastic Neutron Scattering,* Phys. Rev. Lett. **107**, 097401 (2011).

[29] S. Hirose, K. Haruki, A. Ando and T. Kimura, *Mutual control of magnetization and electrical polarization by electric and magnetic fields at room temperature in Y-type $BaSrCo_{2-x}Zn_xFe_{11}AlO_{22}$ ceramics,* Appl. Phys. Lett. **104**, 022907 (2014).

[30] T. Nakajima, Y. Tokunaga, M. Matsuda, S. Dissanayake, J. Fernandez-Baca, K. Kakurai, Y. Taguchi, Y. Tokura and T. Arima*, Magnetic structures and excitations in a multiferroic Y-type hexaferrite $BaSrCo_2Fe_{11}AlO_{22,}$* Phys. Rev. B **94**, 195154 (2016).

[31] See Supplemental Materials for additional details on the magnetic characteristics of the samples, polarization dependence of the electromagnon resonances.

[32] N. Momozawa, Y. Yamaguchi and M. Mita, *Magnetic Structure Change in $Ba_2Mg_2Fe_{12}O_{22,}$* J. Phys. Soc. Jpn. **55**, 1350 (1986).

[33] N. Momozawa, Y. Nagao, S. Utsumi, M. Abe and Y. Yamaguchi, *Cation Distribution and Helimagnetic Structure of the $Ba_2(Zn_{1-x}Mg_x)_2Fe_{12}O_{22}$ System as Revealed by Magnetization Measurements and Neutron Diffraction,* J. Phys. Soc. Jpn. **70**, 2724 (2001).

[34] H. Chang, H. B. Lee, Y.-S. Song, J.-H. Chung, S. A. Kim, I. H. Oh, M. Reehuis and J. Schefer, *Al doping effect on magnetic phase transitions of magnetoelectric hexaferrites $Ba_{0.7}Sr_{1.3}Zn_2(Fe_{1-x}Al_x)_{12}O_{22,}$* Phys. Rev. B **85**, 064402 (2012).

[35] H. B. Lee, S. H. Chun, K. W. Shin, B.-G. Jeon, Y. S. Chai, K. H. Kim, J. Schefer, H. Chang, S.-N. Yun, T.-Y. Joung and J.-H. Chung, *Heliconical magnetic order and field-induced multiferroicity of the Co_2Y-type hexaferrites $Ba_{0.3}Sr_{1.7}Co_2Fe_{12}O_{22,}$* Phys.

Rev. B **86**, 094435 (2012).

[36] J. S. Lee, N. Kida, S. Miyahara, Y. Takahashi, Y. Yamasaki, R. Shimano, N. Furukawa and Y. Tokura, *Systematics of electromagnons in the spiral spin-ordered states of* $RMnO_3$, Phys. Rev. B **79**, 180403(R) (2009).

[37] S. Ishiwata, D. Okuyama, K. Kakurai, M. Nishi, Y. Taguchi and Y. Tokura, *Neutron diffraction studies on the multiferroic conical magnet* $Ba_2Mg_2Fe_{12}O_{22}$, Phys. Rev. B **81**, 174418 (2010).

[38] S. H. Chun, K. W. Shin, H. J. Kim, S. Jung, J. Park, Y.-M Bahk, H.-R. Park, J. Kyoung, D.-H. Choi, D.-S. Kim, G.-S. Park, J. F. Mitchell and K. H. Kim, *Electromagnon with Sensitive Terahertz Magnetochromism in a Room-Temperature Magnetoelectric Hexaferrite*, Phys. Rev. Lett. **120**, 027202 (2018).

[39] Y. Kajiwara, K. Harii, S. Takahashi, J. Ohe, K. Uchida, M. Mizuguchi, H. Umezawa, H. Kawai, K. Ando, K. Takahashi, S. Maekawa and E. Saitoh, *Transmission of electrical signals by spin-wave interconversion in a magnetic insulator*, Nature **464**, 262-266 (2010).

[40] T. Kubacka, J. A. Johnson, M. C. Hoffmann, C. Vicario, S. de Jong, P. Beaud, S. Grübel, S.-W. Huang, L. Huber, L. Patthey, Y.-D. Chuang, J. J. Turner, G. L. Dakovski, W.-S. Lee, M. P. Minitti, W. Schlotter, R. G. Moore, C. P. Hauri, S. M. Koohpayeh, V. Scagnoli, G. Ingold, S. L. Johnson and U. Staub, *Large-Amplitude Spin Dynamics Driven by a THz Pulse in Resonance with an Electromagnon,* Science **343**, 1333-1336 (2014).

Figure captions

FIG1. Magnetic structures and phase diagrams of Y-type hexaferrites $BaSrCo_2Fe_{11}AlO_{22}$ and $Ba_{0.5}Sr_{1.5}Cu_2Fe_{11}AlO_{22}$. (a) The schematics of the crystal structure of the Y-type hexaferrites. Total magnetic moments in the L blocks (red) and the S blocks (green) constitute the L-spins and the S-spins, respectively. Magnetic structures in the $BaSrCo_2Fe_{11}AlO_{22}$ and the $Ba_{0.5}Sr_{1.5}Cu_2Fe_{11}AlO_{22}$ are schematically illustrated in (b), (c) and (d). (b) Alternating longitudinal conical (ALC) structure. (c) Longitudinal conical (LC) and ferrimagnetic (FM) structures under the magnetic field parallel to the c axis ($H_{dc}//c$). (d) Transverse conical (TC) and ferrimagnetic (FM) structures under the magnetic field perpendicular to the c axis ($H_{dc}\perp c$). Phase diagrams for the $BaSrCo_2Fe_{11}AlO_{22}$ in the magnetic field (e) for $H_{dc}//c$ and (f) for $H_{dc}\perp c$ [30]. Phase diagrams for the $Ba_{0.5}Sr_{1.5}Cu_2Fe_{11}AlO_{22}$ in the magnetic field (g) for $H_{dc}//c$ and (h) for $H_{dc}\perp c$ (see Supplemental Material [31]).

FIG. 2. Electromagnon resonance for $BaSrCo_2Fe_{11}AlO_{22}$. (a) Temperature dependence of the electromagnon resonance for three polarization configurations, $E^{\omega}//c$, $H^{\omega}\perp c$ (upper

panel), $E^{\omega}\perp c$, $H^{\omega}//c$ (middle panel) and $E^{\omega}\perp c$, $H^{\omega}\perp c$ (bottom panel), at H_{dc}=0. The electromagnon resonance is excited by the electric field of light polarized along the *c* axis ($E^{\omega}//c$). Magnetic field dependence of the electromagnon spectra ($H_{dc}\perp c$) (b) at 200 K after the field cooling [30] and (c) at 300 K for the light polarization of $E^{\omega}//c$, $H^{\omega}\perp c$. The inset shows the schematics of spin structures under the magnetic field. (d) The magnetization curves at 200 K and at 300 K. The triangles indicate the transitions from the transverse conical (TC) phase to the ferrimagnetic (FM) phase. The inset shows the magnified view at 300 K, which shows the hysteresis behavior between the alternating longitudinal conical (ALC) phase and the TC phase. Magnetic field dependence of the color-coded electromagnon spectra (e) at 200 K and (f) at 300 K. The electromagnon resonance is observed in helical spin phases (ALC and TC) and disappears in the collinear FM phase.

FIG. 3. Magnetochromism by generation of electromagnon resonance ($H_{dc}//c$) for $Ba_{0.5}Sr_{1.5}Cu_2Fe_{11}AlO_{22}$. The evolution of electromagnon (a) at 200 K and (c) at 300 K with increasing magnetic field ($H_{dc}//c$). The polarization of light is $E^{\omega}//c$ and $H^{\omega}\perp c$. The electromagnon resonance shows steep evolution upon the transition from the ALC phase to the LC phase around 2 T. The spectra of electromagnon above the phase transition (b) at 200 K (> 2.05 T) and (d) at 300 K (> 2.5 T). The suppression of the electromagnon resonance is observed with increasing magnetic field. The schematics in (a) and (b) show the transitions of magnetic structure from the ALC phase to the LC phase and from the LC to the FM phase, respectively. (e) The magnetization curves at 200 K and at 300 K. The transitions from the ALC phase to the LC phase, which is

evidenced by the jump of the magnetization, are indicated by triangles. Magnetic field dependence of the color-coded electromagnon spectra (f) at 200 K and (g) at 300 K.

FIG. 4. Large energy shift of electromagnon resonance induced by the magnetic field ($H_{dc}\perp c$) for $Ba_{0.5}Sr_{1.5}Cu_2Fe_{11}AlO_{22}$. The evolution of the electromagnon resonance with increasing magnetic field ($H_{dc}\perp c$, $H_{dc}<$ 3.8 T) (a) at 200 K and (c) at 300 K. The polarization of light is $E^{\omega}//c$ and $H^{\omega}\perp c$. The magnitude and the resonance energy of the electromagnon gradually increase with increasing magnetic field. The magnetic field dependence of electromagnon spectra above 3.8 T (b) at 200 K and (d) at 300 K. The schematics in (c) and (d) show the magnetic structures under the magnetic field. (e) The magnetization curves for $H_{dc}\perp c$ at 200 K and at 300 K. The triangles indicate the transition from the TC phase to the FM phase. Magnetic field dependences of the color-coded electromagnon spectra (f) at 200 K and (g) at 300 K.

FIG. 5. Magnetic field dependence of the spectral weights of the electromagnon (ΔSW) for the $BaSrCo_2Fe_{11}AlO_{22}$ (denoted as BSCoFAO) in $H_{dc}\perp c$, (open circles), and for the $Ba_{0.5}Sr_{1.5}Cu_2Fe_{11}AlO_{22}$ (denoted as BSCuFAO) in $H_{dc}\perp c$ (closed triangles) and in $H_{dc}//c$ (open squares) at (a) 200 K and (b) 300 K. The ΔSW values are deduced from the spectra in Fig. 2, 3 and 4 and see the text for the definition of the ΔSW.

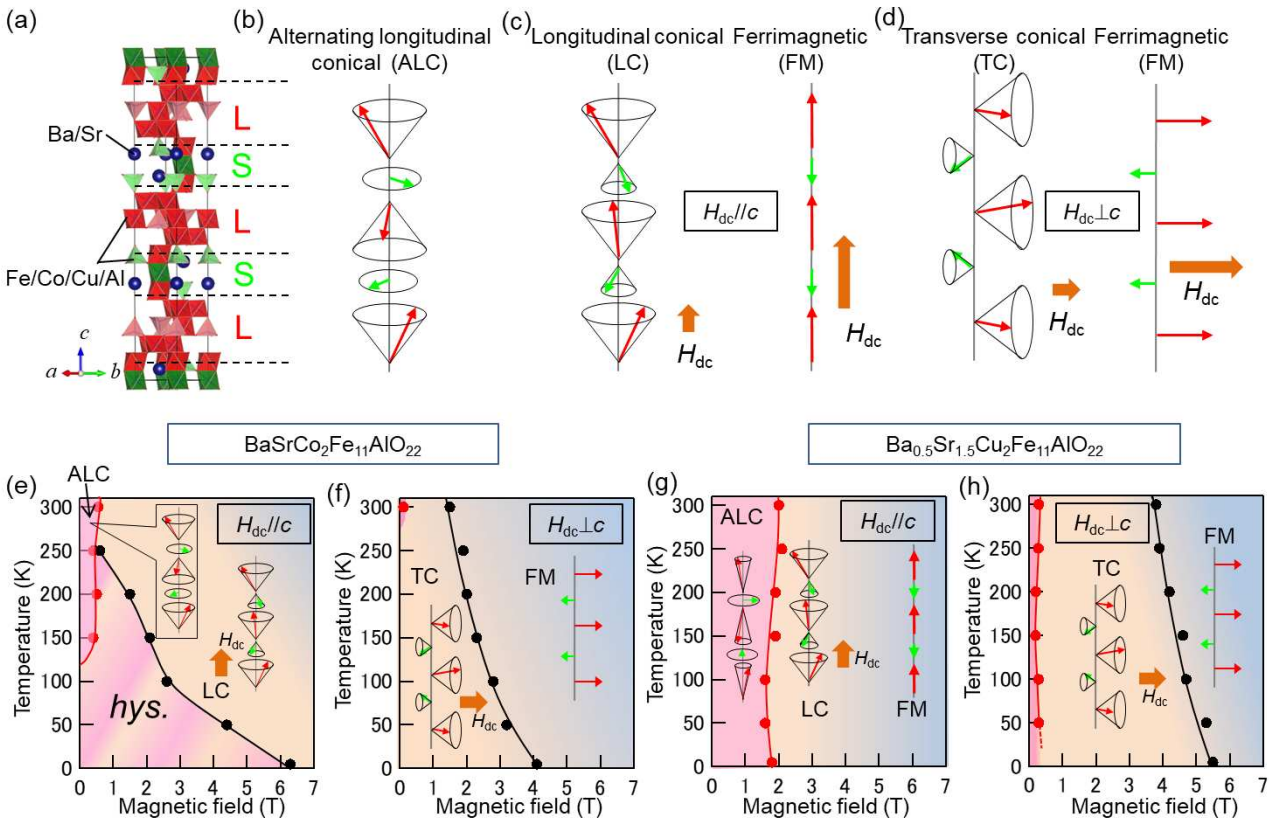

Figure 1 XM10290N 08MAR2018

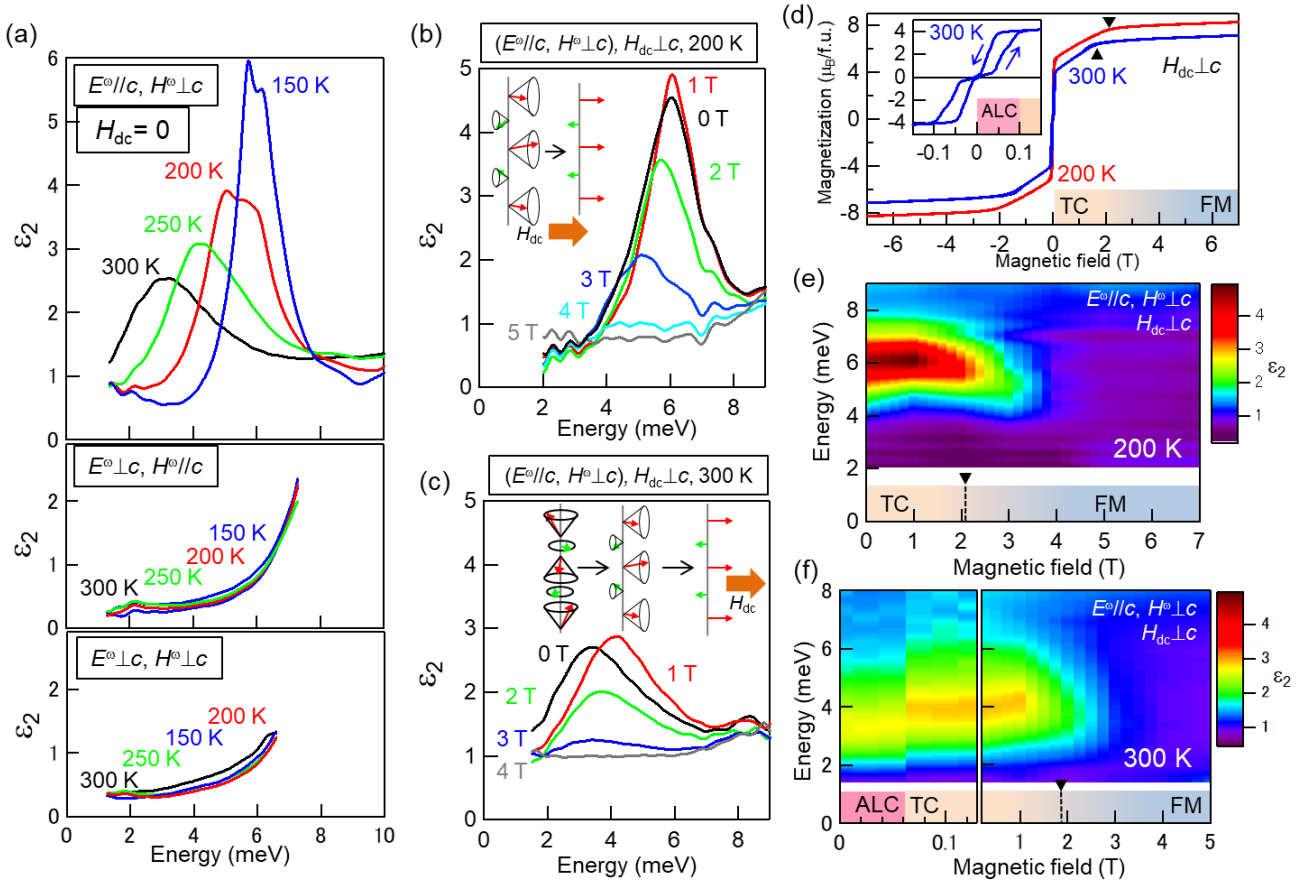

Figure 2 XM10290N 08MAR2018

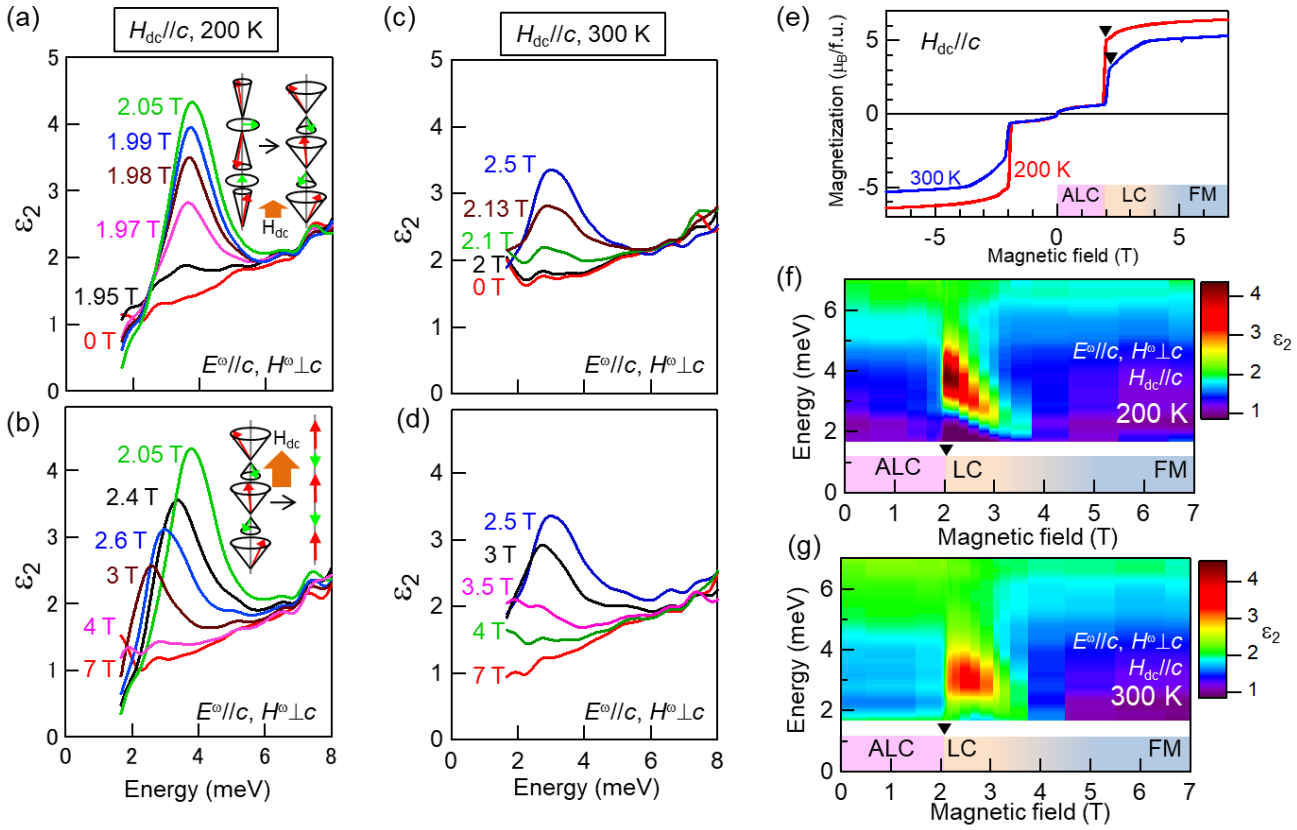

Figure 3 XM10290N 08MAR2018

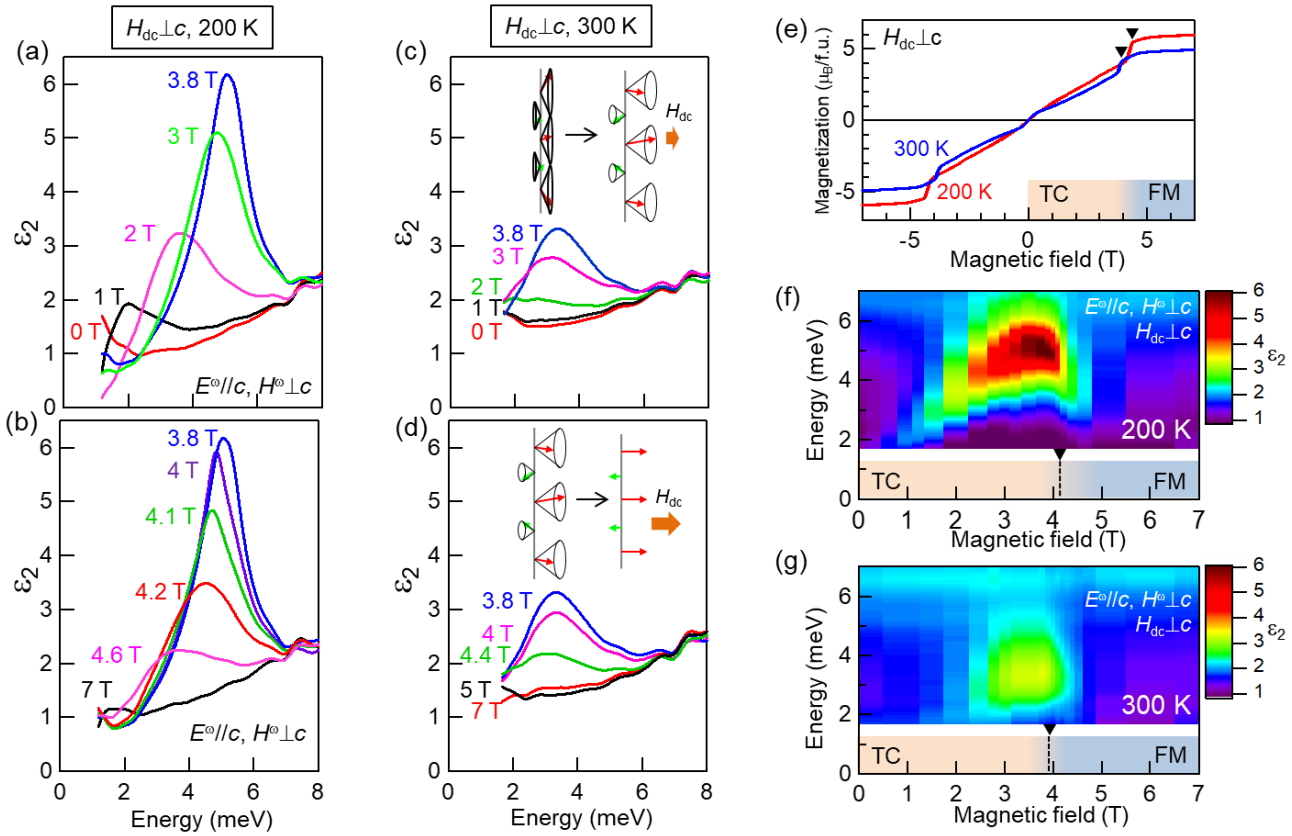

Figure 4 XM10290N 08MAR2018

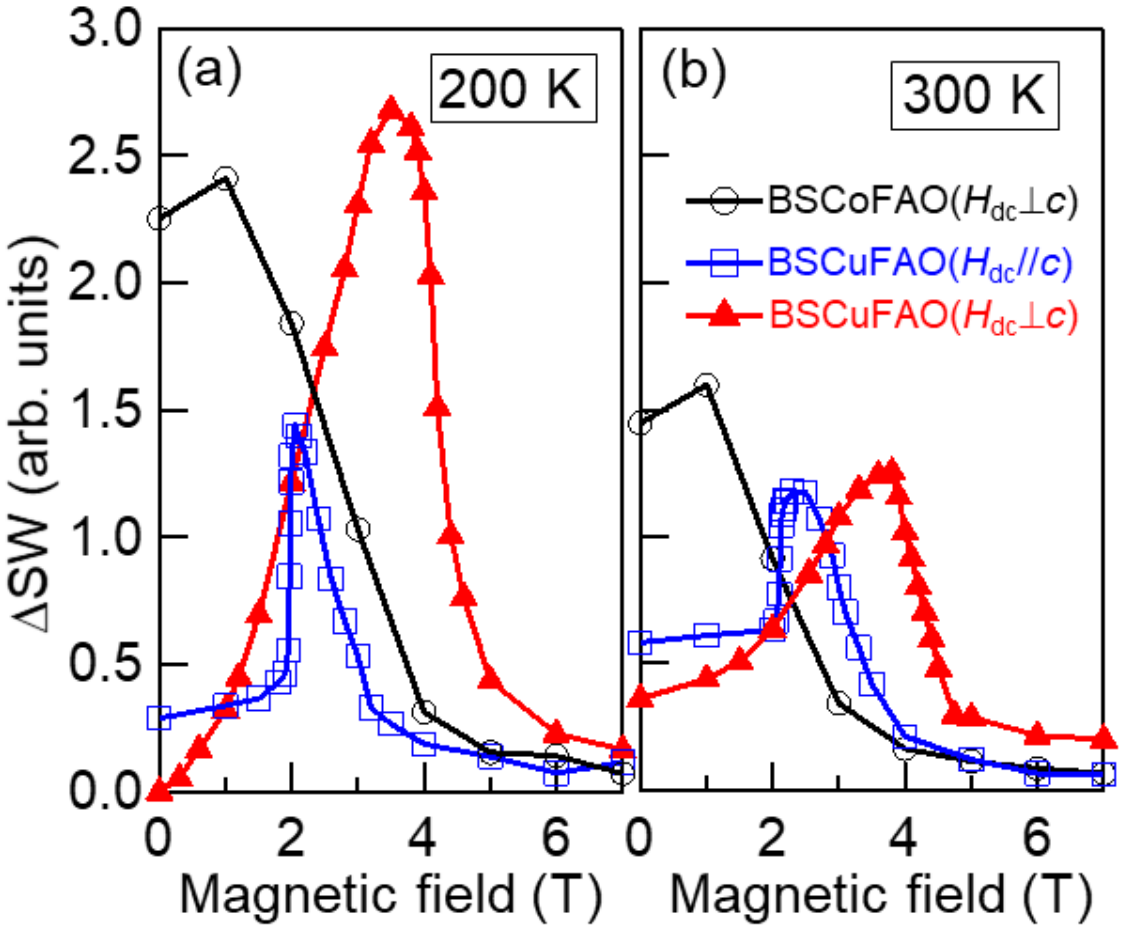

Figure 5 XM10290N 08MAR2018